Materials Today Bio 25 (2024) 101010

Contents lists available at ScienceDirect

Materials Today Bio

journal homepage: www.journals.elsevier.com/materials-today-bio

From static to dynamic: The influence of mechanotransduction on skin equivalents analyzed by bioimaging and RNAseq

Katharina Kaiser [a], Sofie M. Bendixen [a], Jens Ahm Sørensen [b], Jonathan R. Brewer [a,*]

[a] University of Southern Denmark, Department of Biochemistry and Molecular Biology, Campusvej 55, Odense M, 5230, Denmark
[b] Odense University Hospital, Research Unit of Plastic Surgery, Odense C, 5000, Denmark

ARTICLE INFO

Keywords:
Skin-on-a-chip
Artificial skin
Mechanotransduction
Microfluidics

ABSTRACT

In this study, we explore the impact of mechanical stimuli on skin models using an innovative skin-on-a-chip platform, addressing the limitations of conventional transwell-cultured skin equivalents. This platform facilitates cyclic mechanical stimulation through compression and stretching, combined with automated media perfusion. Our findings, using bioimaging and bulk RNA sequencing, reveal increased expression of Keratin 10 and Keratin 14, indicating enhanced skin differentiation and mechanical integrity. The increase in desmosomes and tight junctions, observed through Claudin-1 and Desmoplakin 1 & 2 analysis, suggests improved keratinocyte differentiation due to mechanical stimulation. Gene expression analyses reveal a nuanced regulatory response, suggesting a potential connection to the Hippo pathway, indicative of a significant cellular reaction to mechanical stimuli. The results show the important influence of mechanical stimulation on skin model integrity and differentiation, demonstrating the potential of our microfluidic platform in advancing skin biology research and pharmaceutical testing.

1. Introduction

The skin as the body's largest organ plays an important role in protecting against pathogens, external forces, and other harmful factors [1]. Since the first in vitro skin containing dermal and epidermal layers was developed in 1981 [2], skin-equivalents have been established as useful tools in biological studies and as alternatives to animal testing, and research to increase the morphological relevance of the models has come into focus [3,4]. In recent years, the importance of controlling the spatiotemporal conditions of skin-equivalents has been discussed, as the skin is always exposed to stimuli such as shear stress, stretching, and compression, which are not given in conventional skin-equivalents [5]. More focus has been placed on generating models with different chemical and physical stimuli and so-called Skin-on-a-chip (SOC) models have been designed to establish a finely controlled environment during the cultivation period [5–10]. The main advantage of the SOC technique is the relatively simple and inexpensive method and the ability to successfully reproduce the skin, compared to alternatives such as 3D printing and organoids [11,12].

The skin is constantly exposed to various types of mechanical forces, a phenomenon that has only been considered when developing organotypic skin models in recent years. It has been found that physical stimulation in cell cultures triggers biochemical signaling pathways and the cells respond with modified gene and protein expression, and changes in the differentiation and proliferation of the cells [13–20]. A variety of different 2D cell culture stretching devices have been established, but results from 2D experiments are unlikely to fully depict the processes occurring in vivo since the crosstalk between fibroblasts and keratinocytes and the impact of the 3D micro-environment is not taken into consideration [10,21,22]. In recent years, several skin equivalents have been developed with the aim of testing the effects of mechanical forces on the skin [5,10,11,23–26]. Results observed in these studies varied widely, depending on the stimuli, cell sources, and the matrix scaffold. Specifically, several studies have developed skin equivalents to explore the effects of mechanical forces on skin behavior, utilizing diverse techniques to apply mechanical stress [5,10,11,23–26].

For instance, Mori et al. [5] developed a perfusable and stretchable 3D culture system, while Tokuyama et al. [10] and Kim et al. [11] utilized mechanical stretching to induce changes in skin equivalents. Jung et al. [23] introduced a novel approach combining mechanical stress with air exposure, and Lim et al. [24], along with Varone et al. [25] and Jeong et al. [26], further expanded on these methods with devices

* Corresponding author.
E-mail address: brewer@bmb.sdu.dk (J.R. Brewer).

https://doi.org/10.1016/j.mtbio.2024.101010
Received 22 December 2023; Received in revised form 23 February 2024; Accepted 26 February 2024
Available online 2 March 2024

designed to simulate various mechanical stimuli, including cyclic stretching and mimicking circadian rhythm impacts.

The outcomes of these mechanical stimulations have shown varied effects on skin models, such as changes in epidermal thickness [5], cell proliferation [11], and even signs of aging [24] depending on the method and duration of stress applied. This variation shows the challenge in creating skin models that accurately reflect the dynamic nature of human skin under mechanical forces.

In this study, we assessed the effect of mechanical stimuli in the form of cyclic uniaxial compression and stretching as well as media perfusion on simple skin equivalents composed of a N/TERT-1 keratinocyte cell line and a dermis composed of human dermal fibroblasts and Rat Tail Collagen. The morphology of the skin equivalents was evaluated by H&E staining. After confirming the proper structure of the skin equivalents, bulk RNA sequencing was performed to investigate transcriptome changes. Subsequently, the expression and localization of proteins necessary for maintaining the tissue integrity were characterized using immunofluorescence. Although studies have been conducted on mechanical stress in skin equivalents, most microfluidic platforms employing mechanical stimulation were reliant on gravity-driven media flow and electric-motor-driven actuation. Here, we employ the use of a pneumatically driven mechanical stimulation platform with pump-driven media flow, making it an automated setup without the necessity of frequent media changes.

2. Methods

2.1. Design and manufacturing of stretchable device

A detailed description of the protocol for chip development can be found elsewhere [27]. 3D-printed molds were filled with PDMS base mixed in a ratio of 20:1 with the cross-linking agent and cured for 45 min at 80 °C. The top compartments with the pressure chambers were glued together using a thin layer of PDMS. Inlet and outlet holes were punched using a 2 mm biopsy puncher, and the membrane was sandwiched between the top compartment and.

The bottom channel using silicon glue (MED6215, NuSil), clamped together between two glass slides, and cured for 30 min. Inlet and outlet tubing (PTFE, 1/32″ OD) was attached, and tubing was connected to the pressure chambers. The chip was autoclaved prior to use.

2.2. Cell culture and construction of skin equivalents

HDF were maintained in Dulbecco's Modified Eagle Medium (DMEM) (D0819, Sigma) supplemented with 10% FBS (F7524, Sigma) and 1x Penicillin-Streptomycin (P/S) (15,140, Gibco), and passaged using Trypsin-EDTA. Immortalized N/TERT-1 keratinocytes were grown in Keratinocyte Serum Free Medium (KSFM) (21,068–028, Gibco) supplemented with Human Recombinant Epidermal Growth Factor and Bovine Pituitary Extract (37,000,015, Gibco), 1x P/S, and a final concentration of 0.4 mM CaCl2 (C-34006, Sigma). For passaging, cells were trypsinized and blocked in 45% DMEM, 45% Hams F12, and 10% FBS, followed by pelleting and resuspension in supplemented KSFM. Only cells of passages 2–5 were used to generate the models. To avoid sample contraction the chips were coated with polydopamine as described in Refs. [27,28]. This resulted in covalent bonding between the collagen and the polydopamine on the chip surface, thereby preventing sample contraction. Prior to setting up the models, the well of each chip was functionalized with 1 mg/ml polydopamine in 10 mM Tris (pH 8) for 24 h. The polydopamine was removed and the wells were washed twice with 1x PBS, before drying the chips for 1 h. The gel-neutralizing solution was prepared by mixing 20 μL NaOH (S2770, Sigma) with 30 μL 7.5% Sodium Bicarbonate (S8761, Sigma) and 100 μL EBSS (E7510, Sigma). For full-thickness models, HDF were trypsinized and resuspended in FBS to a concentration of 3×10^6 cells/mL. The gel neutralizing solution, 50 μL of FBS (+ HDF for full-thickness models), and 800 μL Rat tail collagen (3 mg/mL, produced in-house) were mixed and 221 μL were dispensed into each chip. For transwell cell cultures, 250 μL were used per well. The dermis was incubated for 30–45 min to allow the gels to polymerize. For SOCs, the bottom channel was flushed with growth media. Keratinocytes were trypsinized and resuspended in growth media. 3×10^5 cells were added per chip, and 3.36×10^5 cells were added to each transwell. All models were changed to 3D media (60% CnT-Prime Full-thickness 3D Airlift Medium (CnT-PRFTAL5 CELLNTEC) + 40% DMEM (2168–028 Gibco) + 1x P/S) after 2 days, followed by introduction to the ALI after an additional 24 h. For transwell models, a spacer was added to the plate to allow more media to be added to each well and the media was changed three times a week. SOCs were attached to 0.5 μL/min flow on day 3 and the media was replaced twice in the syringe pumps during the growth of the models.

2.3. Cyclic mechanical loading

Dynamic SOCs (dSOC) were attached to a dynamic stimulus on day 6. As described in Ref. [27], Uniaxial mechanical loading was applied with a CETONI Nemesys Syringe Pump at 0.01 Hz and 10% displacement from day 6 onward (stretch and return speed: 5%/sec, compression time: 48 s, relaxation time: 48 s). See figure supplementary figure A1 for more details. As a control, models were grown in transwells to observe the development without dynamic stimulation and without flow (called Transwell FTM), and in the static chip without stimulation but with flow (FTMSOC). The skin equivalents were extracted from the chip and snap-frozen in OCT using 2-methylbutane in liquid nitrogen on day 13. Samples for immunofluorescent labeling and HE staining were sliced into 10 μm sections using a cryotome (Shandon Cryotome, Thermo Fisher).

2.4. Skin samples

The research conducted in this project utilized human skin acquired from surgical operations at Odense University Hospital (OUH), with approval granted by the Southern Denmark Regional Research Ethics Committee. In this study, samples were obtained from three female donors. These included thigh skin from a 27-year-old donor, back skin from a 40-year-old donor, and abdominal skin from a 66-year-old donor. Following initial cleaning, the skin samples were stored at −80 °C. All tissue collections complied with both Danish national laws and the Helsinki Declaration. Ethical clearance for the use of these samples was provided by the Regional Research Ethics Committee of Southern Denmark. Donor identities were kept anonymous, and tissues were obtained after receiving written informed consent.

2.5. Immunofluorescence and histology staining

The slices were fixed in −20 °C Methanol for 15 min, followed by three washing steps in 1 x PBS. For immunofluorescence, the samples were blocked for 30 min in a blocking buffer composed of 1% bovine serum albumin (BSA) (A7030-10G, Sigma-Aldrich) in 1 x PBS. The samples were then incubated overnight at 4 °C with the primary antibody (Cytokeratin 14 (CK14; ab7800, Abcam), Cytokeratin 10 (CK10; ab76318 m Abcam), Desmoplakin (DSP; ab16434, Abcam), Claudin (CLDN; ab180158, Abcam), Ki67 (ab245113, Abcam)) diluted in blocking buffer and washed 3 times in 1x PBS. The secondary antibodies (Alexa Fluor 635 anti-mouse (A31575, Invitrogen) and Abberior STAR 488 anti-rabbit (2-0012-006-5, Abberior) were added, incubated for 1 h at room temperature, and washed three times in 1xPBS. The samples were mounted using Prolong Diamond Antifade Mountant with DAPI (P36962, Invitrogen). The mounted skin slices were imaged using a Nikon A1 confocal microscope with a Plan Apo λ 100× Oil objective. Immunolabelings shown here were acquired in z-stacks with 5 steps and a step size of 0.125 μm. For each step, 3 × 3 fields of view were stitched together with 10% overlap. For analysis purposes, z-stacks were

acquired with a 1 μm step size and a total of 5 steps, and a single field of view. The contrast of the displayed images was individually adjusted using ImageJ to enhance the visualization of structures within the samples. It is important to note that this adjustment was not for qualitative assessment of intensity differences, as a separate quantitative analysis was conducted for that purpose.

For histological analysis, the samples were fixed for 15 min in −20 °C Methanol, stained with hematoxylin and eosin, and mounted in Prolong Antifade Diamond (P36961, Invitrogen). Imaging took place on a Nikon Ti2 widefield microscope with NIS software and a Nikon Andor Zyla monochrome camera. A 60x/1.20 water objective and a 20x/0.75 air objective were used for image acquisition. Three transmitted light images with blue, green, and red filter cubes in the light path were taken to generate the color images.

2.6. Image analysis

Images were analyzed as follows.

2.6.1. Epidermis thickness analysis

To analyze the influence of stretching stimuli on the epidermal layer, the thickness of the epidermal layer was measured in ImageJ. Five images were taken per triplicate using a 20x/0.75 air objective. The thickness was determined by measuring the entire area of the model and dividing it by the length of the basal layer.

2.6.2. Cytokeratin analysis

To analyze the influence of stretching stimuli on cytokeratins, the intensity of Cytokeratin 14 and Cytokeratin 10 was measured. For this, maximum intensity projections were created from images and the mean intensity was measured of a 100 μm area. The analysis was done in ImageJ. In total, three biological replicates were imaged in five different xy positions, and three squares were measured per image (n = 45). The intensity of Cytokeratin 14 and Cytokeratin 10 was measured to analyze the influence of stretching stimuli on cytokeratins.

To see whether stretching and flow have an impact on the cytokeratin distribution throughout the epidermis, ImageJ was used to extract line plots (width of line: 300) across the viable part of the epidermis. Five images were taken per biological triplicate, and 4 line plots were drawn across each image (n = 60). For visualization, the data was normalized in RStudio, and the datasets were binned to 100 values to be able to compare epidermis layers of different thicknesses.

To evaluate the stratification, trapezoidal numerical integration was done on the mean lines produced in the line plots in the range 50–100 of the epidermis. The area between the two curves was calculated and termed the differentiation index.

2.6.3. Proliferation index analysis

The proliferative capacities of the skin equivalents were evaluated by Ki67 labeling. Post image acquisition, the files were analyzed in NIS-Elements Analysis Software using General Analysis 3 (GA3). The channels were processed by shading correction and denoising. The DAPI signal was subsequently thresholded to be able to filter the nuclei. The Ki67-signal in the Cy5.5 channel was detected if it was co-localized in the nuclei. The proliferation index was calculated as follows:

$$Proliferation\ Index = \frac{Ki67 - positive\ cells}{DAPI - positive\ cells}$$

Five images with five z-steps were analyzed per biological triplicate.

2.6.4. Desmoplakin and Claudin analysis

Desmoplakin and Claudin were analyzed by measuring the mean intensity of a line crossing the cell junction of a maximum intensity projection in ImageJ (length 1 μm, width 100 pixels). Five lines were drawn per image and five images were analyzed per biological triplicate (n = 75).

2.7. RNA-isolation and sequencing analysis

To isolate the RNA, a protocol was followed from the RNeasy Mini Kit (74104, Qiagen). Skin equivalents were removed from the transwells and chips and stored in RNAlater (AM7020, Invitrogen) at 4 °C overnight and followed by storage at −20 °C until further use. The full-thickness models were homogenized in the RLT buffer provided in the kit using a p1000 pipette. For the subsequent steps, the protocol in the kit was followed for RNA isolation. The RNA concentration was measured on a NanoDrop spectrophotometer and the quality was analyzed with a Fragment Analyzer 5200 (Agilent). Libraries were constructed using the NEBNext Ultra RNA Library Prep Kit (Illumina, New England Biolabs), and the NovaSeq 6000 platform was used for RNA sequencing. Reads were aligned to the human genome using STAR [29] and DESeq2 [30] was used with default settings in the Next-Generation Sequencing HOMER pipeline. This was done to pinpoint differentially expressed genes. Visualization and statistical analysis were conducted in R.

3. Results

3.1. Generated skin equivalents

In total six different types of skin equivalents were created. An overview can be found in Table 1. Full-thickness equivalents (FTM) were generated by incorporating human dermal fibroblasts (HDF), whereas epidermis equivalents (EM) constituted only of a collagen matrix for the dermal part. Flow was applied on models grown in the fabricated microfluidic platforms (SOC and dSOC), and mechanical stimuli in the form of cyclic mechanical loading were only applied to dynamic chips (dSOC). The cyclic uniaxial compression and stretching of the chip simulates cyclic mechanical loading of the skin, similar to the forces exerted on skin due to the slow bending of a joint. The samples were cycled at a frequency of 0.01 Hz and with a displacement of 10 %, see supplementary figure A1. To avoid sample shrinkage due to collagen contraction, an issue which has confounded multiple skin models [31], the chips were coated with polydopamine as described in Refs. [26,27]. This resulted in tight cohesion of the skin models to the chip due to covalent bonding between the collagen and the polydopamine on the chip surface, leading to negligible or no sample shrinkage. A representative photo of a sample can be seen in supplementary figure A2.

3.2. Histological characterization of models

A full-thickness and an epidermis model were generated under different mechanical stimuli (see Fig. 1). The morphology of the models was evaluated to see if flow solely or flow and mechanical stimuli together affect the epidermis. Representative images of the epidermis can be seen in Fig. 2A. As seen in the figure, the epidermis is made up of several nucleated cell layers covered by the stratum corneum. It was observed that the dermis was firmly attached to the PDA coated membranes. This led to detachment of the epidermis from the dermis during the postprocessing, as shown in supplementary figure A3.

The epidermal thickness of skin equivalents was measured in the H&E stainings by measuring the area of the epidermis in the skin section and dividing it by the length of the basal layer. The results are shown in Fig. 2B. A significant difference could be found in the models subjected to mechanical stimuli (dEMSOC and dFTMSOC) compared to the standard transwell cultures, as well as between SOC and dSOC. A significant change in thickness was found when mechanical stimuli was applied, but no significant change in thickness was measured from the applied flow alone. It was found that the epidermis of the full-thickness models was on average thicker than the epidermis-only counterpart. The thickness of non-compressed equivalents was significantly thicker than native skin. While the thickness of the epidermis in the dFTMSOC showed no significant difference to native skin, the epidermis in the

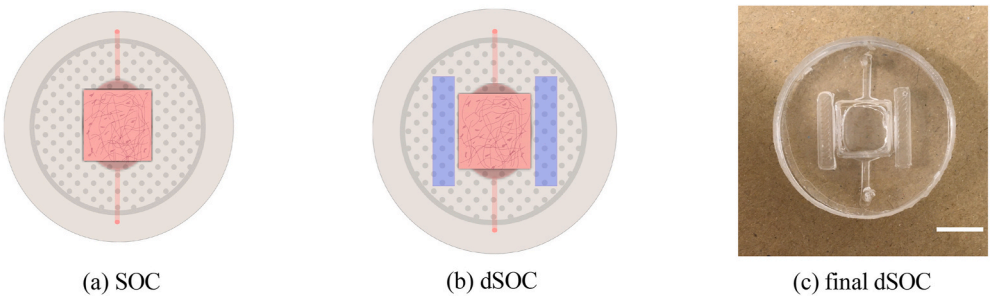

Fig. 1. Design of the microfluidic chips. (a) Drawing of the SOC. (b) Drawing of the dSOC (c) The final dSOC. Figures taken from Ref. [27]. Scale bar: 10 mm.

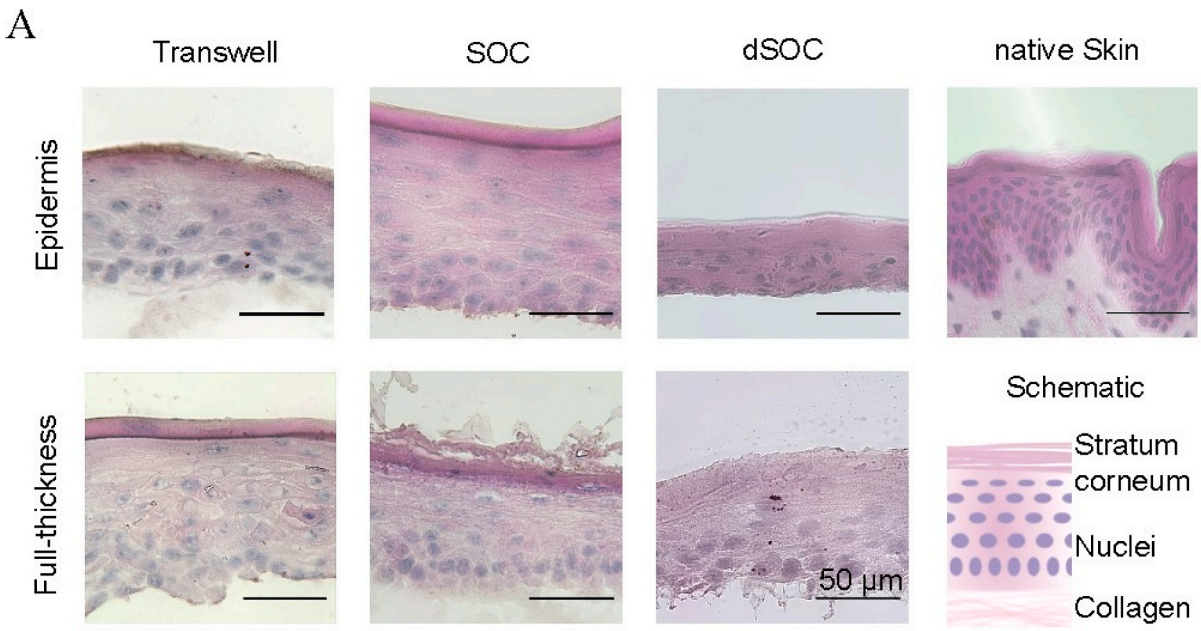

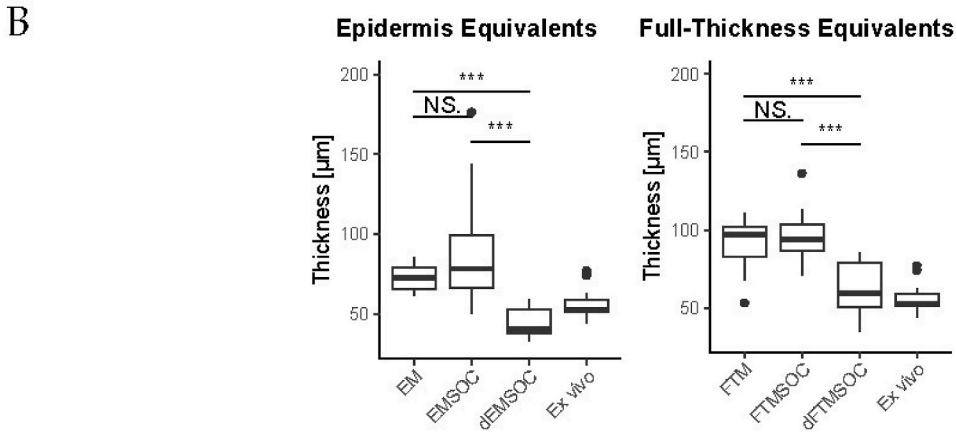

Fig. 2. (A) H&E staining of skin equivalents and native skin. Skin sections of 15 µm thickness were stained with hematoxylin and eosin. Images were acquired using a 60× objective. Images were cropped, rotated, and adjusted for brightness. Scale bars are 50 µm. (B) Analysis of the epidermal thickness of full-thickness and epidermis models. The area of H&E-stained sections was measured and divided by the length of the model using ImageJ to obtain the average thickness. The native skin is an average of the three donors. A Mann-Whitney *U* test was performed on the samples. Data comprises 15 measurements per sample type (3 sample replicates × 5 images). NS $p > 0.05$, *$p \leq 0.05$, **$p \leq .01$, ***$p \leq .001$.

dEMSOC model was significantly thinner than the ex vivo epidermis ($p \leq .001$).

3.3. Differential gene expression and gene ontology analysis

To identify the transcriptional response to mechanical stimulation, we sequenced mRNA from the epidermis and full-thickness models. Epidermis (n = 3) and full-thickness (n = 3) equivalents were grown on

each platform, but due to insufficient RNA isolation of the epidermis equivalents, only the full-thickness samples were analyzed. Analysis of differentially expressed genes (DEGs) revealed differences between FTMSOC and transwell culture, with 2 genes being significantly induced (FDR $\leq$ 0.05) and 23 genes significantly repressed (Fig. 3A).

Additionally, more profound differences were found between dFTMSOC and transwell culture showing 71 and 117 genes significantly induced and repressed, respectively. DEGs for all model-comparisons are shown in Supplementary Materials. Hierarchical clustering of samples revealed similar changes in gene expression between dFTMSOC and FTMSOC, setting them both apart from the transwell culture (Fig. 3B). This was further visualized by a total of 19 shared genes being regulated between dFTMSOC and FTMSOC, leaving only 6 uniquely regulated FTMSOC DEGs (Fig. 3C).

Clustering of the total 194 genes that changed significantly across the FTM equivalents (FDR $\leq$ 0.05) revealed two clusters; one composed of significantly down-regulated genes (blue, n = 121) and one of significantly up-regulated genes (red, n = 73) compared to transwell culture (Fig. 4A). Of these, 98 and 71 genes were found to be dFTMSOC-specific in the down- and up-DEG cluster, respectively, illustrating the more profound differences found for dFTMSOC vs. transwell culture. All 19 shared genes present in FTMSOC and dFTMSOC were found to be down-regulated, indicating, to some extent, a common transcriptional program across conditions.

To elucidate the main processes driven by mechanical stimulation, we performed a gene ontology (GO) analysis (FDR $\leq$ 0.05) of the shared [19], down-dFTMSOC-specific (98), and up-dFTMSOC-specific (71) genes (Fig. 4B). Due to the limited number of FTMSOC-specific DEGs, no analysis was performed for these gene-groups. For the shared and down-dFTMSOC-specific genes it was found that they were enriched for processes mainly associated with inflammation. Among the down-dFTMSOC-specific processes, type I interferon regulation, cell differentiation, and regulation of response to external stimulus were enriched, containing genes such as *STAT1* (Signal Transducer and Activator of Transcription 1), *VEGFA* (Vascular Endothelial Growth Factor A), *F2* (Coagulation Factor II, Thrombin), *IFIT*1-3 and 5 (Interferon-Induced Protein with Tetratricopeptide Repeats 1–3 and 5) and *CXCL10* (C-X-C Motif Chemokine Ligand 10). In addition, Anion transmembrane transport was found to be significant only forthe down-dFTMSOC genes, containing genes like *SLC4A11* (Solute Carrier

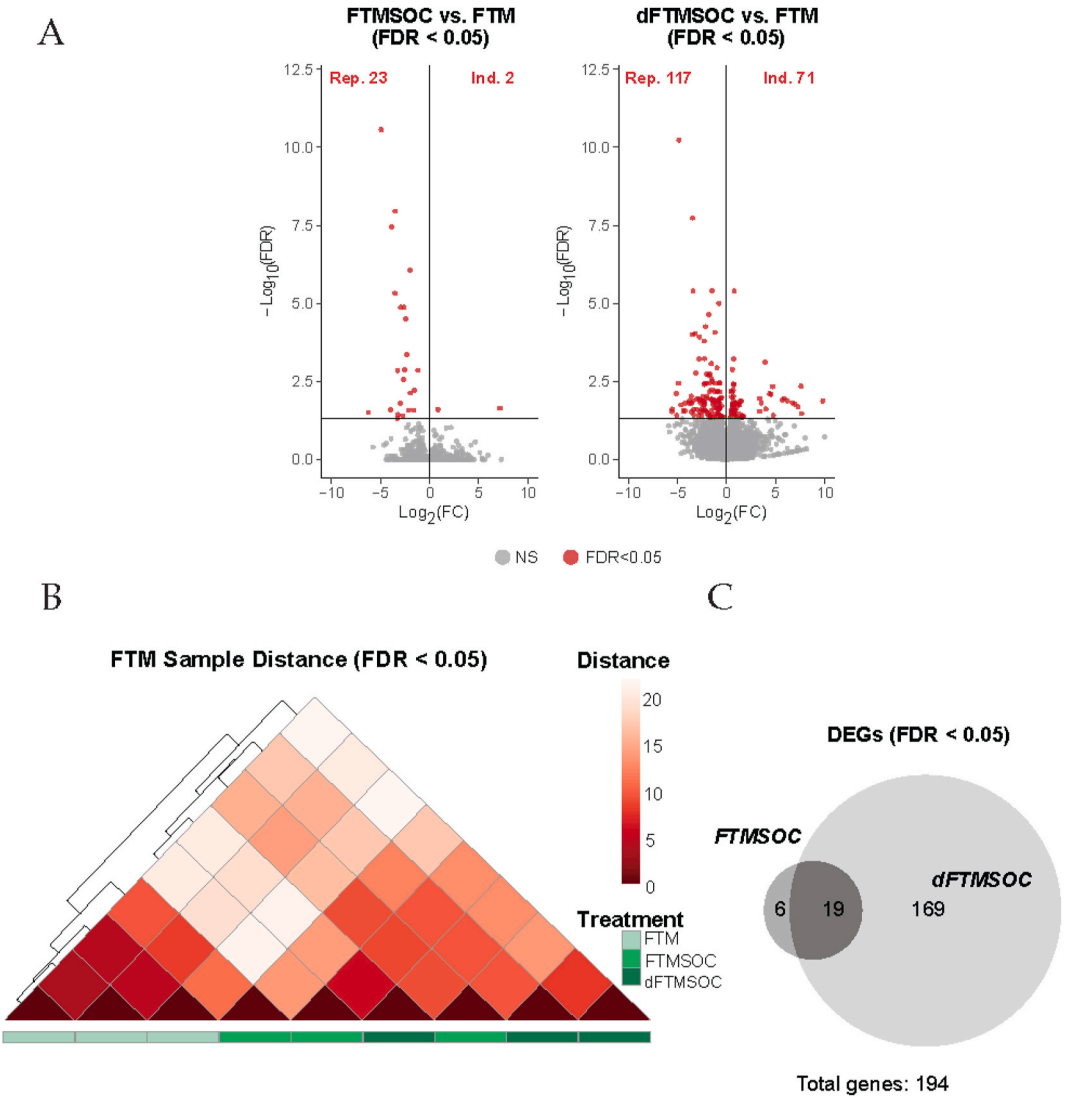

Fig. 3. Transcriptional changes upon mechanical stimuli. (A) Log2FC of all expressed genes in FTM conditions related to transwell culture. Significantly induced and repressed genes (FDR $\leq$ 0.05) are shown in red with indication of gene numbers. (B) Distance plot of FTM equivalents based on all DEGs (FDR $\leq$ 0.05) found between (d)FTMSOC and transwell culture. (C) Venn diagram of 19 shared genes between FTMSOC and dFTMSOC experiments (FDR $\leq$ 0.05). DEG, differentially expressed genes; FDR, false discovery rate; FC, fold change. (For interpretation of the references to colour in this figure legend, the reader is referred to the Web version of this article.)

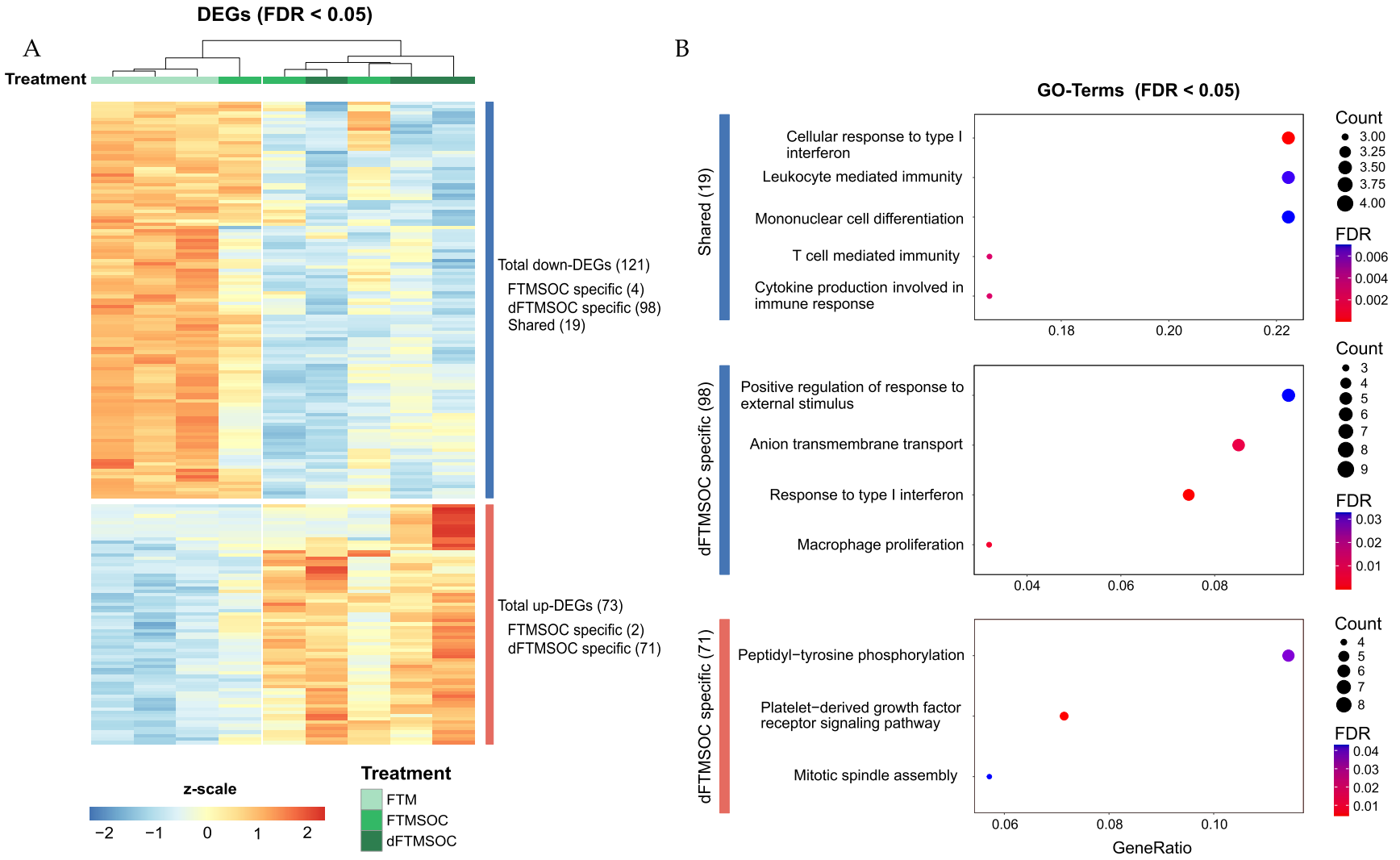

Fig. 4. (A) Scaled mean expression of 194 DEGs across FTMSOC and dFTMSOC experiments. Clusters are colored based on up- (red) or down- (blue) regulated genes compared to transwell culture. The number of up- or down-regulated DEGs is noted in parentheses. (B) Selected GO terms enriched among shared (blue), down-dFTMSOC-specific (blue), and up-dFTMSOC-specific (red) DEGs. DEG counts within categories (circles) and FDR (color) are shown. DEG, differentially expressed genes; FDR, false discovery rate; GO, Gene Ontology. (For interpretation of the references to colour in this figure legend, the reader is referred to the Web version of this article.)

Family 4 Member 11) and *SLC12A9* (Solute Carrier Family 12 Member 9), both important for maintaining cellular ion balance and volume.

We further found the GO analyses of the up regulated dFTMSOC-specific DEGs as being enriched for cell-regulatory processes such as peptidyltyrosine phosphorylation (*PTPN11* (Protein Tyrosine Phosphatase, Non-Receptor Type 11) and *VTN* (Vitronectin)), platelet-derived growth factor receptor signaling pathway (*CBL* (Casitas B-Lineage Lymphoma), *FER* (Fer Kinase) and *RDX* (Radixin)), and mitotic spindle assembly (*KIF2A* (Kinesin Family).

Overall, we identified transcriptional changes in response to mechanical stimulation across full-thickness equivalents with genes associated with immune-related processes being significantly down regulated and genes associated with cell-regulatory processes being significantly up regulated compared to transwell culture.

3.4. Immunofluorescence of models

After observing changes in gene expression in the models due to perfusion and uniaxial mechanical stimuli, the next step was to evaluate changes in protein expression and localization. To ensure that the models developed properly, antibody labeling with Cytokeratin 14 (CK14), Cytokeratin 10 (CK10), Desmoplakin 1 & 2 (DSP1&2), Claudin 1 (CLDN1), and Ki67 was performed.

The expression of CK14 and CK10 in reconstructed skin was found to resemble that of ex vivo skin. While CK10 expression was confined to the suprabasal layers in all models, CK14 was found in the basal cell layer, confirming the proper differentiation of the epidermal keratinocytes (see Fig. 5A) [32].

An intensity analysis based on the immunolabeling was performed to draw conclusions about the expression of CK14 and CK10 in static models vs. flow and dynamic models (Fig. 5B). A significant difference could be found between static models grown in transwells and models grown in SOC or dSOC for both CK14 and CK10. No significant difference in protein expression could be found between models grown in SOC and models grown in dSOC, except for the CK14 expression in the epidermis model.

To study the distribution of CK14 and CK10 throughout the epidermis, lines were drawn through the viable epidermis from the basal layer to the apical side. The intensity plots were normalized to a range of 0–1 and binned to a length of 100 to allow a comparison of the intensity

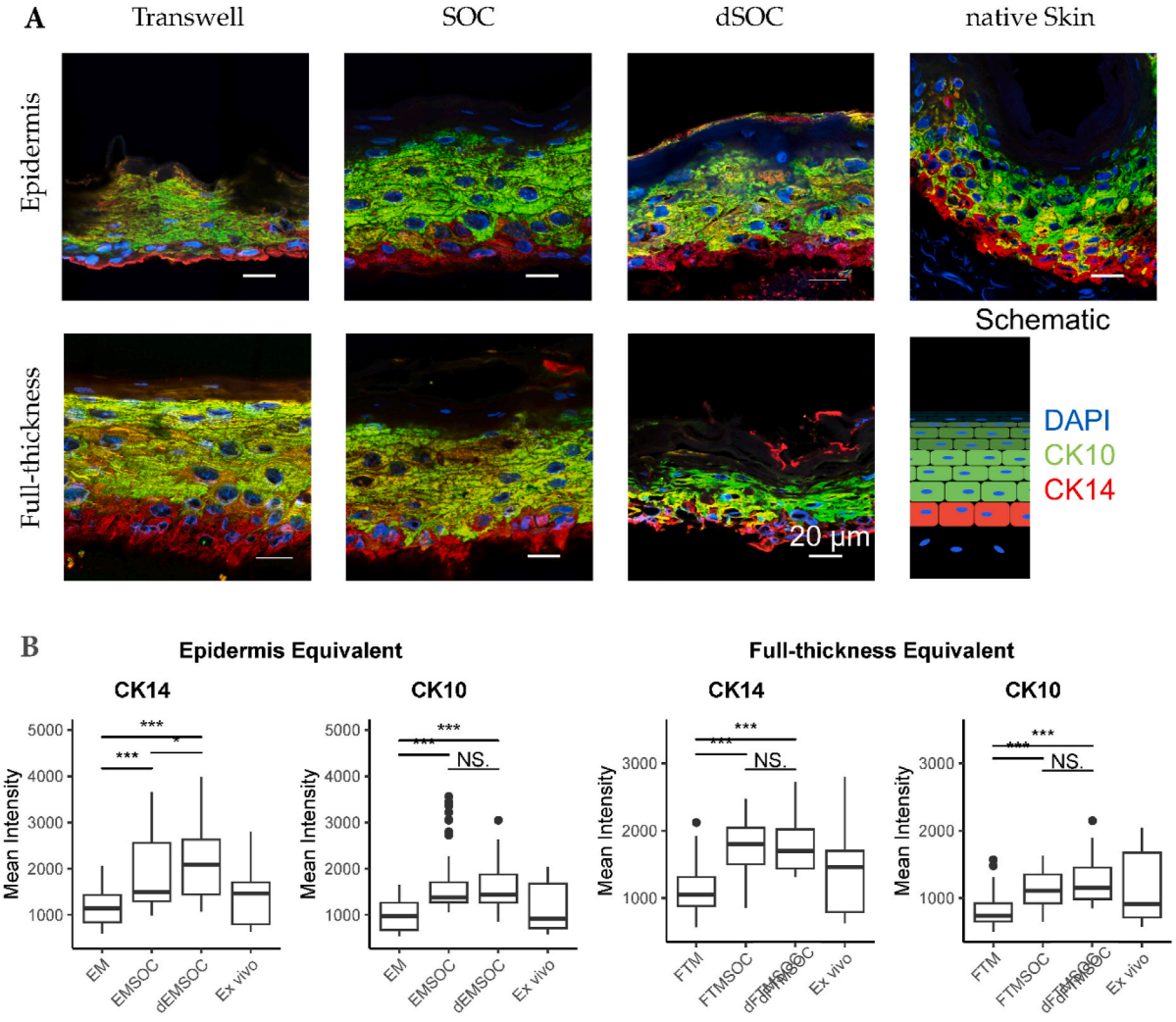

Fig. 5. (A) Immunolabeling of Cytokeratin 10 and 14 in epidermal and full-thickness skin equivalents. Organotypic cultures grown under different conditions were cut into 15 µm sections on a cryotome and immunolabelled for CK10 and CK14. Nuclei were stained using DAPI. Images shown are deconvolved maximum intensity projections of stacks, which were cropped, rotated and contrast adjusted for optimal visualization. The stratum corneum is oriented towards the top of the field of view and the basal cell layer is located at the bottom. The intensity of the images is adjusted to visualize the structures. Scale bars are 20 µm. (B) Intensity analysis of CK14 and CK10. Maximum intensity projections were created, and the mean intensity of a 100 µm2 square was measured. Three biological replicates were imaged five times, and 3 squares were measured per image. The ex vivo data is an average of the three donors. Data consists of 45 measurements per sample type (3 sample replica × 5 images x 3 regions of interest). A Mann-Whitney *U* test was performed on the samples. NS $p > 0.05$, *$p \leq .05$, **$p \leq .01$, ***$p \leq .001$.

according to the position in the epidermis. The mean and standard deviation of the normalized and binned datasets are plotted in Fig. 6. Native skin showed a bigger difference in the expression of CK14 and CK10 in the upper viable layers compared to the models. It appears that the relative intensity of CK10 increases sooner in models without dynamic stretching, as a plateau is reached before reaching 50% of the epidermal layer. CK14 expression is found in the basal layer, and all the way up into the apical direction in all models.

The keratin differentiation index based on the line plot analysis showed an increase in differentiation in SOC and dSOC cultivated skin equivalents. It was found that native skin had a higher degree of keratin differentiation than the skin equivalents.

Labeling of DSP1 & 2 and CLDN1 showed the location of the desmosomes and validated the proper formation of tight junctions (see Fig. 7). The mean intensity of maximum intensity projections of cell junctions was measured for both DSP1&2 and CLDN1 by drawing a line across the cell junction (length 1 μm, width 100 pixels). Five lines were drawn per image. A higher mean intensity of CLDN1 was found in dEMSOC compared to EM and EMSOC. In full-thickness models, a slight increase in CLDN1 was found in FTMSOC compared to FTM, and the intensity in dFTMSOC was higher than in FTMSOC. Analysis of DSP 1 & 2 showed a statistical difference between the static cultures and the mechanically stimulated dSOC, as well as between SOC and dSOC cultures. However, interestingly, no difference was observed between the epidermal and full-thickness models. (see Fig. 8).

The proliferation marker Ki67 was detected in all viable layers of the epidermis in all models (see supplementary Figure A4). A GA3 analysis was performed in NIS Analysis software to determine the proliferation index. The nuclei were counted for DAPI and Ki67, and the ratio of Ki67-positive nuclei to DAPI-stained nuclei was calculated.

It was found that the application of flow significantly changed the proliferation index for both epidermis equivalents and full-thickness equivalents (see Fig. 9). A comparison of SOC and dSOC showed significant differences for epidermis equivalents, whereas no significant difference could be found in full-thickness equivalents. A closer look at the expression of Ki67 in native skin revealed statistical differences in the proliferation index between the three ex vivo samples ($p < 0.001$). A boxplot comparing the data for the different skin origins is attached in supplementary Figure A5 (see Table 1).

A summary of the main results can be found collected in Table 2.

4. Discussion

This study aimed to evaluate the effect of flow and dynamic cyclic mechanical stimuli on reconstructed skin. The thickness of the epidermis of the fabricated models was measured and compared. It was found that equivalents grown on SOC devices exhibited no significant change in epidermal thickness compared to conventional transwell cultures. The application of mechanical stimuli resulted in a significant decrease in thickness compared to those in static transwell cultures. These findings correlate to results published by Jeong et al., who discovered a significant decrease in epidermal thickness by compressive stimulation [26]. Our observations are contrary to the increases in epidermal thickness observed in stretched skin models by other researchers [5,10]. This may be due to the mode of stimulation, as previously discussed by Kim et al. [11].

However, it is important to consider which forces are applied to the cells during the cyclic mechanical loading. Assuming a constant cell volume, initial compression results in cell deformation. As the cell is compressed along the compression axes it expands (ie. is stretched) along the perpendicular axes to conserve volume. This is indicative of both compressive and tensile forces during compression. Similarly, subsequent relaxation or uniaxial stretching of the skin applies tensile forces in the direction of displacement and compressive forces in

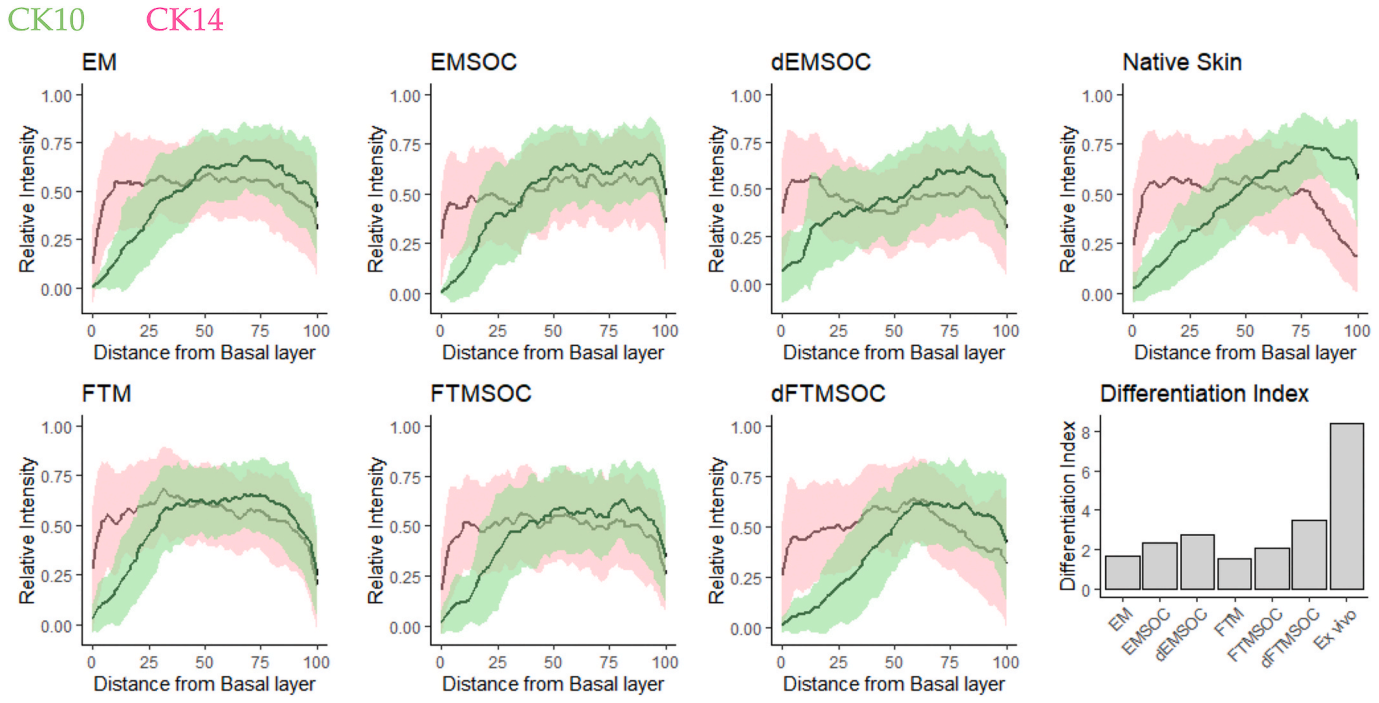

Fig. 6. Line plot analysis of CK10 and CK14 and the calculated Keratin Differentiation Index. Line plots were drawn (width of line: 300) for maximum intensity projections, the intensity was normalized, and the distance was binned to fit on a scale from 0 to 1 and 0 to 100 respectively. X-axis shows the relative distance from the bottom of the basal layer and Y-axis shows the relative intensity. CK14 is shown in light pink and CK10 is shown in green. The line presents the mean, the shaded area shows the standard deviation. Three lines were drawn per image, and five images were taken for each biological triplicate. Keratin Differentiation Index. Trapezoidal numerical integration was performed on the lines. For each sample type, the area between CK14 and CK10 expression was calculated for the suprabasal layers of the epidermis to determine the differentiation level. (For interpretation of the references to colour in this figure legend, the reader is referred to the Web version of this article.)

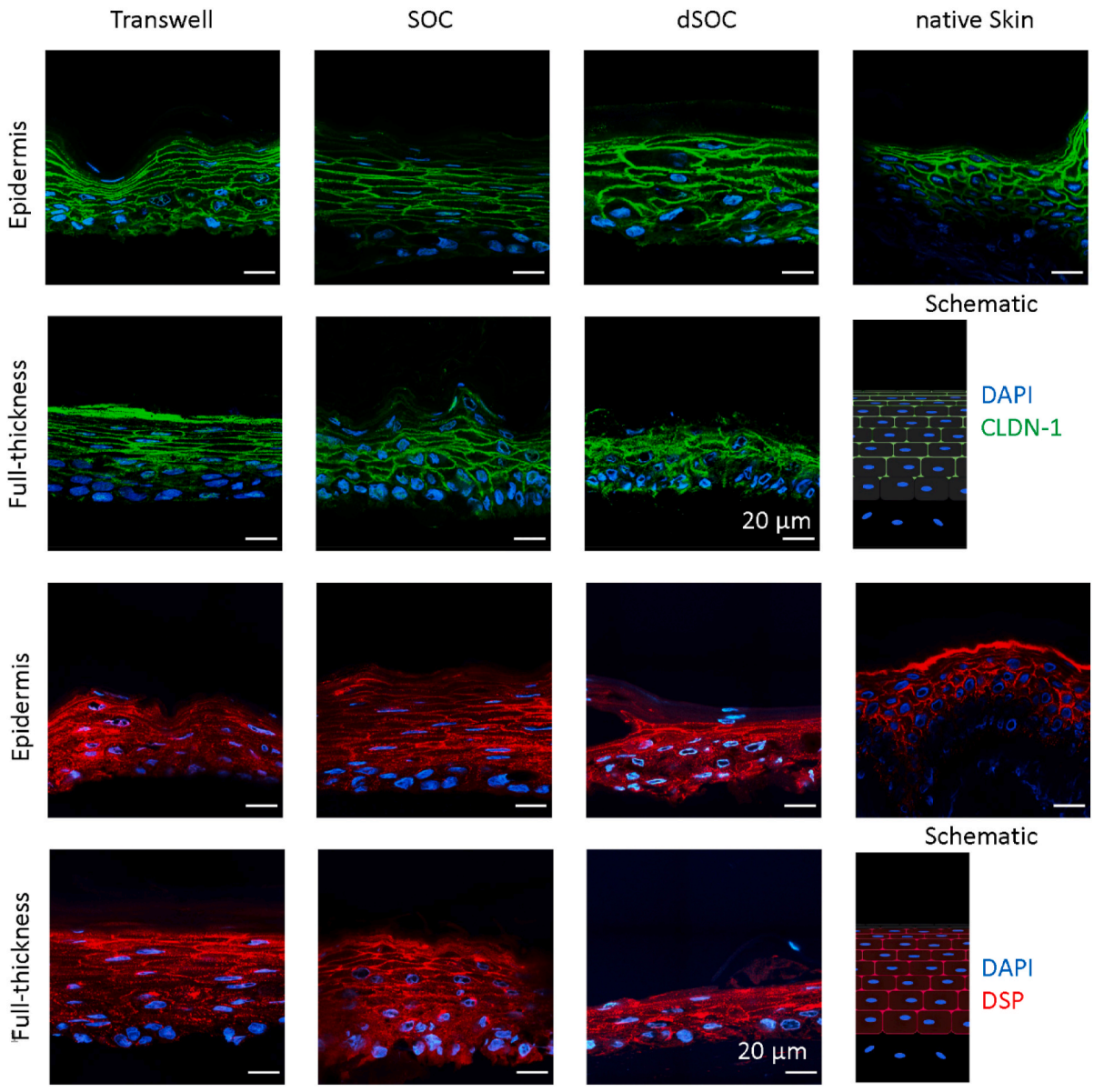

Fig. 7. Immunolabeling of DSP 1 & 2 (RED) and CLDN1 (GREEN) in epidermal and full-thickness skin equivalents. Organotypic cultures grown under different conditions were cut into 15 µm sections on a cryotome and immunolabelled. Nuclei were stained using DAPI. Images were acquired using a 100× objective and the shown figures are deconvolved maximum intensity projections of stacks, which were cropped and rotated for better visualization. The stratum corneum is oriented towards the top of the field of view and the basal cell layer is located at the bottom. The contrast of the images is adjusted to visualize the structures. Scale bars are 20 µm. (For interpretation of the references to colour in this figure legend, the reader is referred to the Web version of this article.)

perpendicular directions. It is also interesting to consider what is to be defined as the resting state for the skin models which are exposed to cyclic loading for prolonged intervals. As the skin model adapts to the stimuli over time the most relaxed state would be an intermediate position not one of the extremes. This would correspond to in the case of an elbow that the resting position would be when the arm is slightly bent. In summary, these observations suggest that in experiments involving prolonged cyclic loading, different initial displacement directions (stretching or compression) may impart similar mechanical stimuli. Therefore, the variations observed could be attributable to other experimental factors, such as the specific skin models used.

The next aim was to observe changes in gene expression in our equivalents as a result of dynamic perfusion and mechanical stress. Bulk RNAseq revealed differences in the gene expression between models grown on the microfluidic platform and models grown on conventional transwell systems. More profound differences were seen for dFTMSOC compared to transwell culture than for FTMSOC. This elucidate that the transcriptome profiles may be more profoundly altered by mechanical stimulation than flow. Upregulated DEGs were mostly involved in cell-regulatory processes, whereas downregulated DEGs were involved in immune-related processes.

The shared genes that were found to be down-regulated in both FTMSOC and dFTMSOC compared to the static transwell were associated with GO-terms such as cytokine production, the cellular response to interferon-1, and leukocyte and T cell-mediated immunity suggest a general suppression of genes related to cellular stress in skin grown on microfluidic chips compared to those cultivated in transwells [33,34]. This might indicate reduced cellular stress due to enhanced cellular function in dynamic culture conditions. Such improvements could arise because the chips with flow more closely emulate human physiological conditions, as previously suggested in other models [35,36].

The downregulated of genes related to the "cellular response to type I

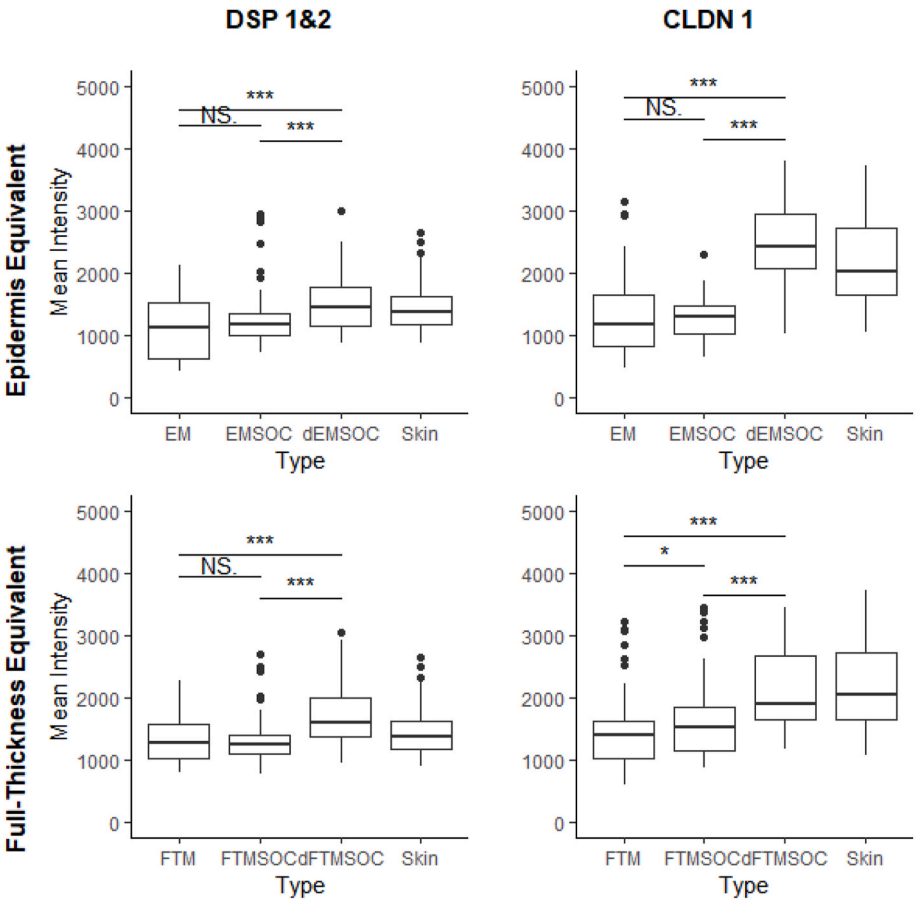

Fig. 8. Intensity analysis of CLDN1 and DSP1&2. Maximum intensity projections were created, and the mean intensity of the tight junctions and desmosomes was measured. Three biological replicates were imaged five times, and 5 spots were measured per image. The ex vivo data is an average of the three donors. Data consists of 75 measurements per sample type (3 sample replica × 5 images x 5 regions of interest). A Mann-Whitney *U* test was performed on the samples. NS $p > 0.05$, *$p \leq 0.05$, **$p \leq .01$, ***$p \leq .001$.

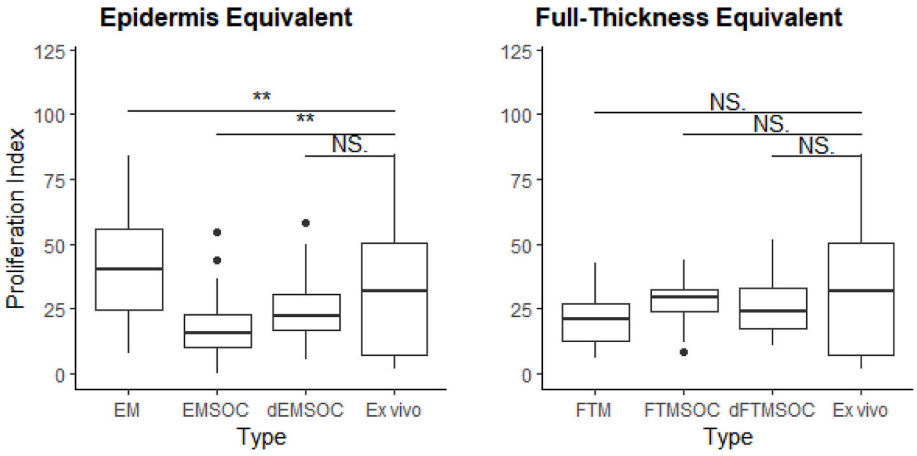

Fig. 9. Proliferation Index. Ki67-positive nuclei and DAPI-stained nuclei were counted, and the percentage of Ki67-positive nuclei was calculated. Three biological replicates were imaged five times. The ex vivo data is an average of the three donors. A Mann-Whitney *U* test was performed on the samples. NS $p > 0.05$, *$p \leq 0.05$, **$p \leq .01$, ***$p \leq .001$.

interferon" found in dFTMSOC suggests a decrease in inflammatory responses [37]. Keratinocytes in healthy skin have been shown to constitutively express interferons at a basal level, allowing for rapid induction of interferon signaling if needed [38,39]. A decrease in this process could suggest a slower response time to inflammation in dFTMSOC cultures, however, this would need to be tested in the future.

Furthermore, the down-regulation of genes related to the "anion *trans*-membrane transport" could be related to a controlled response to maintain ion balance, cell volume, and skin barrier properties [40]. It is also important to note that these processes most likely involve both keratinocytes in the epidermis and fibroblasts in the dermis, contributing to overall tissue response [41].

Table 1
Overview over fabricated skin equivalents.

Sample	Abbreviation	Platform	HDF	Flow	Mechanical stimuli
Epidermis Model	EM	Transwell			
Epidermis-on-a-chip	EMSOC	SOC		✓	
dynamic Epidermis-on-a-chip	dEMSOC	dSOC		✓	✓
Full-thickness Model	FTM	Transwell	✓		
Full-thickness-on-a-chip	FTMSOC	SOC	✓	✓	
dynamic Full-thickness-on-a-chip	dFTMSOC	dSOC	✓	✓	✓

In terms of mechanotransduction, development, and proliferation, the upregulation of peptidyltyrosine phosphorylation, along with the gene TEAD1, a key protein in the Hippo pathway, was observed. While peptidyl-tyrosine phosphorylation is known to activate multiple signaling pathways [42], it is, together with *TEAD1*, involved in the Hippo pathway [43]. This pathway is known to facilitate mechanotransduction in skin, controlling tissue development, proliferation, and homeostasis [44,45]. Taken together this could suggest that the mechanical stimulation of the skin models activates a response in the cells be mediated by the Hippo pathway.

Additionally, the observed up-regulation of the "mitotic spindle assembly" process lends support to heightened cell division rates, likely aiding tissue repair and regeneration processes in response to the mechanical stress [46,47]. Conversely, the down-regulation of genes related to the "positive regulation of response to external stimulus" implies a regulatory mechanism that curtails excessive responses to mechanical stress, potentially to prevent overactivation. Similarly, the down-regulation of the "response to type 1 interferon" pathway suggests a balance between moderating immune responses and avoiding overactivity, which could lead to excessive inflammation triggered by mechanical stimuli [48].

The results of the RNAseq data in the context of mechanical stimulation of the skin indicate a complex cellular response involving both up-regulation and down-regulation of processes that promote tissue development and repair, as well as mechanisms that ensure controlled and balanced reactions. The results suggest that these processes work together to strike a balance between tissue development and proliferation, while simultaneously implementing regulatory mechanisms to prevent over activity, maintain homeostasis and structural integrity [49].

To our knowledge, DESeq analysis has not been done on mechanically stimulated skin equivalents. Others have previously measured gene expression by real-time quantitative PCR [11,26]. In these studies, the groups found an increase in gene expression for equivalents grown with compressive stimulation, but an overall decrease in equivalents grown under tensile stimulation. In the present study, a higher number of DEG was found to be downregulated, despite the compressive stimulation.

It is interesting to note the observed reduction in immune and stress responses due to prolonged mechanical stimuli. This observation might suggest a form of regulatory control, wherein mechanical cues, after some time of stimulation, lead to a dampened immune or stress response. Such regulation could be a mechanism to avoid overactivation or to maintain tissue homeostasis under healthy dynamic conditions. Further research in this area is necessary to understand how mechanical stimulation can modulate immune responses in the skin. This could have significant implications for treating skin diseases, particularly those characterized by excessive or chronic inflammation.

Immunofluorescence evaluation of CK14, CK10, DSP1&2, CLDN1, and Ki67 showed localization similar to that of native skin tissue. Expression of CK14 in the basal layer and CK10 in the suprabasal layers indicated a proper differentiation of the keratinocytes. Keratin is critical for tissue integrity, as the filaments can withstand mechanical forces well. Differences in the intensity of keratins could be found for models grown on the chip compared to conventional transwell culture. Interestingly, an increase in CK14 expression was found in dEMSOC models compared to EMSOC, but no significant difference in CK10 expression in EMSOC and dEMSOC culture could be found. No significant changes in CK14 and CK10 expression could be found for dFTMSOC and FTMSOC cultures. This could point towards increased production of CK14 and CK10 due to the application of flow. This will have to be investigated further. The distribution of CK14 and CK10 showed a higher epidermal keratin differentiation in the upper strata of native skin compared to the skin equivalents. The results also showed that flow and mechanical stimuli can increase the keratin differentiation in the upper epidermis.

Analysis of DSP1&2 and CLDN1 showed a significant increase in intensity in dSOC models compared to SOC and transwell culture. No significant difference was found between transwell and SOC culture, except for an increase in the intensity of CLDN1 in FTMSOC compared to FTM. This increase of CLDN1 in full-thickness equivalents correlates with results published by Strüver et al., who observed an increase in CLDN1 in perfused full-thickness culture [50]. Further investigations need to take place to determine why we found differences between full-thickness and epidermis-only models. Their group used a flow of 1.25–7.5 ml per hour compared to 30 μL per hour in our setup. The results suggest that the perfusion of the skin equivalent was not enough to affect tight junction and desmosome formation in epidermis-only models, and that the increase in tight junctions might be mediated by fibroblasts. In contrast, no difference was observed for the DSP1&2 intensity between the epidermal and full-thickness models, indicating that the crosstalk between keratinocytes and fibroblasts does not play a significant role in their expression. Other similar studies have indicated that perfusion and mechanical stimuli applied to skin equivalents can lead to the development of a more mature basement membrane [10,50]. This finding is interesting in light of the epidermal detachment from the dermis observed in our postprocessing phase. A more mature basement membrane would typically suggest improved connectivity between the dermis and epidermis. However, the detachment observed in our experiments has not been seen in similar transwell skin culture experiments that did not use PDA [51]. This implies that the detachment may be specifically facilitated by the models binding to the PDA-coated chips/membranes. Although detachment represents a drawback, the use of PDA is crucial as it ensures that the models remain flat and securely in place during mechanical stimulation.

Measuring the proliferation index revealed a significant decrease in proliferation in epidermis equivalents grown on the dynamic platform compared to transwell culture but revealed the opposite in full-thickness models. It was found that the EM sample had a larger variance compared

Table 2
Overview of results. Shown are statistically significant changes compared to the static transwell system. In case of no statistically significant difference, a " = " is shown.

Sample	Platform	Thickness	CK14	CK10	CLDN1	DSP1&2	Proliferation Index
EMSOC	SOC	=	↑	↑	=	=	↓
dEMSOC	dSOC	↓	↑	↑	↑	↑	↓
FTMSOC	SOC	=	↑	↑	↑	=	↑
dFTMSOC	dSOC	↓	↑	↑	↑	↑	↑

to the other skin equivalents, which could indicate a less mature skin equivalent. The analysis of ex vivo skin samples from different body sites and origins revealed significant differences between the three samples (see supplementary Figure A5), explaining the large range displayed in Fig. 9B. Others have previously reported numbers ranging from 10 % to 37.2 % in the stratum basale, all the way to 46% for labeling noted in the basal and the three first suprabasal layers [52–57]. This variation found in the literature supports the wide span of proliferation found in the native skin samples and shows the general variability found between human skin samples.

As noted earlier, the effects of mechanical stimulation on skin models have varied, leading to changes in epidermal thickness [5], cell proliferation [11], and aging signs [24], influenced by the cell and model used as well as the type and length of stress applied. This diversity together with the results in the present study, emphasizes the complexity in developing skin models that truly mimic human skin's response to mechanical stimuli and suggests a need for systematic studies, employing various well-defined stimuli and durations, to better understand these dynamics.

5. Conclusion

In this study, full-thickness and epidermis skin equivalents were generated under static and dynamic growth conditions to observe the impact of automated media flow and mechanical stimuli on the samples. The generated skin equivalents exhibit several advantages over traditional transwell cultures, such as a more realistic microenvironment with perfusion and mechanical stimulation, and a controlled environment. The microfluidic platform allows for a more automated culturing process and offers the potential to replace animal models in the future.

The fabricated skin equivalents exhibit a structure and protein localization similar to native skin and we found that dynamic media perfusion increased keratins expression. We also noted a decrease in epidermal thickness as a result of mechanical stimulation. Furthermore, RNA sequencing analysis revealed a downregulation of genes related to cellular stress in the dynamically cultured samples with automated media flow. This suggests that the dynamic conditions may contribute to improved cellular function in the skin equivalents. The results revealed a significant impact of mechanical stimulation on the skin models, affecting both gene expression and protein levels. Specifically, we observed a notable alteration in gene expression patterns, characterized by a complex interplay in up- and down-regulation of genes related to maintaining tissue homeostasis compared to transwell cultured samples. Specifically, up-regulation of key genes related to the Hippo pathway were found suggesting that the mechanical stimulation of the skin models activates a response in the cells mediated by this pathway. Furthermore, the immunofluorescence results indicated improved differentiation of keratin and an increase in the expression of tight junction and desmosomal proteins in response to dynamic mechanical stimuli. Collectively, these findings suggest that mechanical stimuli mediate an increase in the mechanical integrity of the samples, and this could be facilitated by the Hippo pathway.

Although the skin equivalents developed in this study exhibit limited functionality, owing to their simple design in terms of cell sourcing and scaffold choice, they mark a significant advancement towards developing biomimetic artificial skin. Growing these equivalents under dynamic conditions has enhanced our understanding of mechanical interactions in skin models. Future work is needed to create more complex equivalents to validate the findings obtained from these initial models.

Additional information

The data and analysis required to reproduce the RNAseq findings presented her are available to download from https://doi.org/10.17632/m2wj5gzm6v.1. The data used for the image analysis is available on reasonable request.

CRediT authorship contribution statement

Katharina Kaiser: Writing – original draft, Visualization, Methodology, Investigation, Data curation, Conceptualization. **Sofie M. Bendixen:** Writing – review & editing, Visualization, Data curation. **Jens Ahm Sørensen:** Writing – review & editing, Resources. **Jonathan R. Brewer:** Writing – review & editing, Supervision, Resources, Project administration, Funding acquisition, Formal analysis, Conceptualization.

Declaration of competing interest

The authors declare that they have no known competing financial interests or personal relationships that could have appeared to influence the work reported in this paper.

Data availability

The data and analysis required to reproduce the RNAseq findings presented her are available to download from DOI: 10.17632/m2wj5gzm6v.1. The data used for the image analysis is available on request.

Acknowledgments

This work was supported by grants from the Leo Foundation (LF–OC–19-000219) Foundation and the Novo Nordisk Foundation (NNF19OC0056962). Image acquisition and image analyses were performed at the Danish Molecular Biomedical Imaging Center (DaMBIC, University of Southern Denmark), supported by the Novo Nordisk Foundation (NNF18SA0032928). The N/TERT-1 cell line was provided by Prof. Dr. Ellen van den Bogard, Radboud UMC, the Netherlands.

Appendix A. Supplementary data

Supplementary data to this article can be found online at https://doi.org/10.1016/j.mtbio.2024.101010.

References

[1] A.V. Rawlings, C.R. Harding, Moisturization and skin barrier function, Dermatol. Ther. 17 (2004) 43–48.
[2] E. Bell, H.P. Ehrlich, D.J. Buttle, T. Nakatsuji, Living tissue formed in vitro and accepted as skin-equivalent tissue of full thickness, Science 211 (1981) 1052–1054.
[3] F. Groeber, M. Holeiter, M. Hampel, S. Hinderer, K. Schenke-Layland, Skin tissue engineering — in vivo and in vitro applications, Adv. Drug Deliv. Rev. 63 (2011) 352–366.
[4] A. Houcine, A. Delalleau, S. Heraud, B. Guiraud, B. Payre, H. Duplan, M.-B. Delisle, O. Damour, S. Bessou-Touya, How biophysical in vivo testing techniques can be used to characterize full thickness skin equivalents, Skin Res. Technol. 22 (2016) 284–294.
[5] N. Mori, Y. Morimoto, S. Takeuchi, Perfusable and stretchable 3d culture system for skin- equivalent, Biofabrication 11 (2018) 011001.
[6] C.F.E. Jones, S. Di Cio, J.T. Connelly, J.E. Gautrot, Design of an integrated microvascularized human skin-on-a-chip tissue equivalent model, Front. Bioeng. Biotechnol. 10 (2022).
[7] H.E. Abaci, Z. Guo, A. Coffman, B. Gillette, W.-h. Lee, S.K. Sia, A.M. Christiano, Human skin constructs with spatially controlled vasculature using primary and ipsc-derived endothelial cells, Adv. Healthcare Mater. 5 (2016) 1800–1807.
[8] S. Salameh, N. Tissot, K. Cache, J. Lima, I. Suzuki, P.A. Marinho, M. Rielland, J. Soeur, S. Takeuchi, S. Germain, et al., A perfusable vascularized full-thickness skin model for potential topical and systemic applications, Biofabrication 13 (2021) 035042.
[9] G. Sriram, M. Alberti, Y. Dancik, B. Wu, R. Wu, Z. Feng, S. Ramasamy, P. L. Bigliardi, M. Bigliardi-Qi, Z. Wang, Full-thickness human skin-on-chip with enhanced epidermal morphogenesis and barrier function, Mater. Today 21 (4) (2018) 326–340.
[10] E. Tokuyama, Y. Nagai, K. Takahashi, Y. Kimata, K. Naruse, Mechanical stretch on human skin equivalents increases the epidermal thickness and develops the basement membrane, PLoS One 10 (2015).

[11] K. Kim, S. Jeong, G.Y. Sung, Effect of periodical tensile stimulation on the human skin equivalents by magnetic stretching skin-on-a-chip (mssc), BioChip Journal 16 (2022) 501–514.
[12] J.H. Sung, Y. Wang, M.L. Shuler, Strategies for using mathematical modeling approaches to design and interpret multi-organ microphysiological systems (mps), APL Bioeng. 3 (2019) 021501.
[13] M. Kurita, M. Okazaki, T. Fujino, A. Takushima, K. Harii, Cyclic stretch induces upregulation of endothelin-1 with keratinocytes in vitro: possible role in mechanical stress-induced hyperpigmentation, Biochem. Biophys. Res. Commun. 409 (2011) 103–107.
[14] S. Oh, H. Chung, S. Chang, S.-H. Lee, S.H. Seok, H. Lee, Effect of mechanical stretch on the dncb-induced proinflammatory cytokine secretion in human keratinocytes, Sci. Rep. 9 (2019) 5156.
[15] F. Renò, V. Traina, M. Cannas, Mechanical stretching modulates growth direction and mmp-9 release in human keratinocyte monolayer, Cell Adhes. Migrat. 3 (2009) 239–242.
[16] D. Deng, W. Liu, F. Xu, Y. Yang, G. Zhou, W.J. Zhang, L. Cui, Y. Cao, Engineering human neo-tendon tissue in vitro with human dermal fibroblasts under static mechanical strain, Biomaterials 30 (2009) 6724–6730.
[17] C. Huang, K. Miyazaki, S. Akaishi, A. Watanabe, H. Hyakusoku, R. Ogawa, Biological effects of cellular stretch on human dermal fibroblasts, J. Plast. Reconstr. Aesthetic Surg. 66 (2013) e351–e361.
[18] C.A. Derderian, N. Bastidas, O.Z. Lerman, K.A. Bhatt, S.-E. Lin, J. Voss, J. W. Holmes, J.P. Levine, G.C. Gurtner, Mechanical strain alters gene expression in an in vitro model of hypertrophic scarring, Ann. Plast. Surg. 55 (2005) 69–75.
[19] K. Nishimura, P. Blume, S. Ohgi, B.E. Sumpio, The effect of different frequencies of stretch on human dermal keratinocyte proliferation and survival, J. Surg. Res. 155 (2009) 125–131.
[20] H. Wen, P.A. Blume, B.E. Sumpio, Role of integrins and focal adhesion kinase in the orientation of dermal fibroblasts exposed to cyclic strain, Int. Wound J. 6 (2009) 149–158.
[21] H. Kamble, M.J. Barton, M. Jun, S. Park, N.-T. Nguyen, Cell stretching devices as research tools: engineering and biological considerations, Lab Chip 16 (2016) 3193–3203.
[22] L. Huang, P.S. Mathieu, B.P. Helmke, A stretching device for high-resolution live-cell imaging, Ann. Biomed. Eng. 38 (2010) 1728–1740.
[23] M. Jung, S.-M. Jung, H. Shin, Co-stimulation of hacat keratinization with mechanical stress and air-exposure using a novel 3d culture device, Sci. Rep. 6 (2016) 33889.
[24] H.Y. Lim, J. Kim, H.J. Song, K. Kim, K.C. Choi, S. Park, G.Y. Sung, Development of wrinkled skin-on-a-chip (wsoc) by cyclic uniaxial stretching, J. Ind. Eng. Chem. 68 (2018) 238–245.
[25] A. Varone, J.K. Nguyen, L. Leng, R. Barrile, J. Sliz, C. Lucchesi, N. Wen, A. Gravanis, G.A. Hamilton, K. Karalis, C.D. Hinojosa, A novel organ-chip system emulates three- dimensional architecture of the human epithelia and the mechanical forces acting on it, Biomaterials 275 (2021) 120957.
[26] S. Jeong, J. Kim, H.M. Jeon, K. Kim, G.Y. Sung, Development of an aged full-thickness skin model using flexible skin-on-a-chip subjected to mechanical stimulus reflecting the circadian rhythm, Int. J. Mol. Sci. 22 (2021).
[27] K. Kaiser, J.A. Sørensen, J.R. Brewer, Novel chip for applying mechanical forces on human skin models under dynamic culture conditions, Tissue Eng Part C Methods (2023), https://doi.org/10.1089/ten.TEC.2023.0195.
[28] M. Dabaghi, S. Shahriari, N. Saraei, K. Da, A. Chandiramohan, P. R. Selvaganapathy, J.A. Hirota, Surface modification of pdms-based microfluidic devices with collagen using polydopamine as a spacer to enhance primary human bronchial epithelial cell adhesion, Micromachines 12 (2021).
[29] A. Dobin, C.A. Davis, F. Schlesinger, J. Drenkow, C. Zaleski, S. Jha, P. Batut, M. Chaisson, T.R. Gingeras, STAR: ultrafast universal RNA-seq aligner, Bioinformatics 29 (2012) 15–21.
[30] M.I. Love, W. Huber, S. Anders, Moderated estimation of fold change and dispersion for RNA-seq data with deseq2, Genome Biol. 15 (2014) 1–21.
[31] C. Lotz, F.F. Schmid, E. Oechsle, M.G. Monaghan, H. Walles, F. Groeber-Becker, Crosslinked collagen hydrogel matrix resisting contraction to facilitate full-thickness skin equivalents, ACS Appl. Mater. Interfaces 9 (2017) 20417–20425. PMID: 28557435.
[32] E. van den Bogaard, D. Ilic, S. Dubrac, M. Tomic-Canic, J. Bouwstra, A. Celli, T. Mauro, Perspective and consensus opinion: good practices for using organotypic skin and epidermal equivalents in experimental dermatology research, J. Invest. Dermatol. 141 (2021) 203–205.
[33] J.W. Griffith, C.L. Sokol, A.D. Luster, Chemokines and chemokine receptors: positioning cells for host defense and immunity, Annu. Rev. Immunol. 32 (2014) 659–702.
[34] J. Zhu, H. Yamane, W.E. Paul, Differentiation of effector cd4 t cell populations, Annu. Rev. Immunol. 28 (2009) 445–489.
[35] Y.-C. Toh, T.C. Lim, D. Tai, G. Xiao, D. van Noort, H. Yu, A microfluidic 3d hepatocyte chip for drug toxicity testing, Lab Chip 9 (2009) 2026–2035.
[36] Q. Wu, J. Liu, X. Wang, L. Feng, J. Wu, X. Zhu, W. Wen, X. Gong, Organ-on-a-chip: recent breakthroughs and future prospects, Biomed. Eng. Online 19 (2020) 1–19.
[37] S.V. Kotenko, G. Gallagher, V.V. Baurin, A. Lewis-Antes, M. Shen, N.K. Shah, J. A. Langer, F. Sheikh, H. Dickensheets, R.P. Donnelly, Ifn-λs mediate antiviral protection through a distinct class ii cytokine receptor complex, Nat. Immunol. 4 (2003) 69–77.
[38] C. Conrad, M. Gilliet, Type i ifns at the interface between cutaneous immunity and epidermal remodeling, J. Invest. Dermatol. 132 (2012) 1759–1762.
[39] G.A. Hile, J.E. Gudjonsson, J.M. Kahlenberg, The influence of interferon on healthy and diseased skin, Cytokine 132 (2020) 154605.
[40] L. Ebihara, P. Acharya, J.-J. Tong, Mechanical stress modulates calcium-activated-chloride currents in differentiating lens cells, Front. Physiol. 13 (2022) 814651.
[41] V.W. Wong, M.T. Longaker, G.C. Gurtner, Seminars In Cell & Developmental Biology, vol. 23, Elsevier, 2012, pp. 981–986.
[42] T. Hunter, Tyrosine phosphorylation: thirty years and counting, Curr. Opin. Cell Biol. 21 (2009) 140–146.
[43] N. Reuven, M. Shanzer, Y. Shaul, Hippo Pathway Regulation by Tyrosine Kinases, Springer New York, New York, NY, 2019, pp. 215–236.
[44] E. Rognoni, G. Walko, The roles of yap/taz and the hippo pathway in healthy and diseased skin, Cells 8 (2019) 411. Published 2019 May 3.
[45] J. Wang, Y. Zhang, N. Zhang, C. Wang, T. Herrler, Q. Li, An updated review of mechanotransduction in skin disorders: transcriptional regulators, ion channels, and micrornas, Cell. Mol. Life Sci. 72 (2015) 2091–2106.
[46] C.E. Walczak, R. Heald, Mechanisms of mitotic spindle assembly and function, Int. Rev. Cytol. 265 (2008) 111–158.
[47] T. Wittmann, A. Hyman, A. Desai, The spindle: a dynamic assembly of microtubules and motors, Nat. Cell Biol. 3 (2001) E28–E34.
[48] N. Kopitar-Jerala, The role of interferons in inflammation and inflammasome activation, Front. Immunol. 8 (2017) 873.
[49] J. Andrae, R. Gallini, C. Betsholtz, Role of platelet-derived growth factors in physiology and medicine, Genes Dev. 22 (2008) 1276–1312.
[50] G. Muniraj, R.H.S. Tan, Y. Dai, R. Wu, M. Alberti, G. Sriram, Microphysiological modeling of gingival tissues and host-material interactions using gingiva-on-chip, Adv. Healthcare Mater. 12 (2023) 2301472.
[51] N.D. Jakobsen, K. Kaiser, M.F. Ebbesen, L. Lauritsen, M.F. Gjerstorff, J. Kuntsche, J. R. Brewer, The ROC skin model: a robust skin equivalent for permeation and live cell imaging studies, Eur. J. Pharmaceut. Sci. 178 (2022).
[52] K. Strüver, W. Friess, S. Hedtrich, Development of a perfusion platform for dynamic cultivation of in vitro skin models, Skin Pharmacol. Physiol. 30 (2017) 180–189.
[53] S. Gibbs, A.N. Silva Pinto, S. Murli, M. Huber, D. Hohl, M. Ponec, Epidermal growth factor and keratinocyte growth factor differentially regulate epidermal migration, growth, and differentiation, Wound Repair Regen. 8 (2000) 192–203.
[54] N.A. Coolen, M. Verkerk, L. Reijnen, M. Vlig, A.J. Van Den Bogaerdt, M. Breetveld, S. Gibbs, E. Middelkoop, M.M. Ulrich, Culture of keratinocytes for transplantation without the need of feeder layer cells, Cell Transplant. 16 (2007) 649–661.
[55] W.H. Yap, T.Y. Cheah, L.C. Yong, S.R. Chowdhury, M.H. Ng, Z. Kwan, C.K. Kong, B.-H. Goh, Fibroblast-derived matrices-based human skin equivalent as an in vitro psoriatic model for drug testing, J. Biosci. 46 (2021) 1–13.
[56] C.A. Stewart, R.T. Dell'orco, Age related decline in the expression of proliferating cell nuclear antigen in human diploid fibroblasts, Mech. Ageing Dev. 66 (1992) 71–80.
[57] P. Rousselle, E. Gentilhomme, Y. Neveux, Markers of Epidermal Proliferation and Differentiation, Springer Cham, 2017, pp. 407–415.